Mon. Not. R. Astron. Soc. **425,** 709–719 (2012) doi:10.1111/j.1365-2966.2012.21581.x

A unique isolated dwarf spheroidal galaxy at $D = 1.9$ Mpc

Dmitry Makarov,[1]★ Lidia Makarova,[1] Margarita Sharina,[1] Roman Uklein,[1] Anton Tikhonov,[2]† Puragra Guhathakurta,[3] Evan Kirby[4] and Natalya Terekhova[5]

[1]*Special Astrophysical Observatory, Nizhniy Arkhyz, Karachai-Cherkessia 369167, Russia*
[2]*Astronomical Institute, St Petersburg State University, Universitetskii pr. 28, 198504 St Petersburg, Stary Peterhof, Russia*
[3]*UCO/Lick Observatory, University of California-Santa Cruz, Santa Cruz, CA 95064, USA*
[4]*Department of Astronomy, California Institute of Technology, 1200 East California Boulevard, MC 249-17, Pasadena, CA 91125, USA*
[5]*Sternberg Astronomical Institute, Moscow State University, Universitetsky pr. 13, Moscow 119991, Russia*

Accepted 2012 June 23. Received 2012 June 11; in original form 2012 April 9

ABSTRACT

We present a photometric and spectroscopic study of the unique isolated nearby dwarf spheroidal (dSph) galaxy KKR 25. The galaxy was resolved into stars with *Hubble Space Telescope*/Wide Field Planetary Camera 2 including old red giant branch and red clump. We have constructed a model of the resolved stellar populations and measured the star formation rate and metallicity as a function of time. The main star formation activity period occurred about 12.6–13.7 Gyr ago. These stars are mostly metal poor, with a mean metallicity [Fe/H] ~ -1 to -1.6 dex. About 60 per cent of the total stellar mass was formed during this event. There are indications of intermediate-age star formation in KKR 25 between 1 and 4 Gyr with no significant signs of metal enrichment for these stars. Long-slit spectroscopy was carried out using the Russian 6-m telescope of the integrated starlight and bright individual objects in the galaxy. We have discovered a planetary nebula (PN) in KKR 25. This is the first known PN in a dSph galaxy outside the Local Group. We have measured its oxygen abundance $12 + \log(\mathrm{O/H}) = 7.60 \pm 0.07$ dex and a radial velocity $V_\mathrm{h} = -79$ km s^{-1}. We have analysed the stellar density distribution in the galaxy body. The galaxy has an exponential surface brightness profile with a central light depression. We discuss the evolutionary status of KKR 25, which belongs to a rare class of very isolated dwarf galaxies with spheroidal morphology.

Key words: galaxies: distances and redshifts – galaxies: dwarf – galaxies: individual: KKR 25 – galaxies: stellar content.

1 INTRODUCTION

The isolated dwarf spheroidal (dSph) galaxy KKR 25 was discovered by Karachentseva, Karachentsev & Richter (1999) during the search of dwarf galaxies in the direction of the Local Void. Follow-up observations with the 100-m radio telescope at Effelsberg (Huchtmeier, Karachentsev & Karachentseva 2000, 2003) have shown H I emission in the object with a radial velocity $V_\mathrm{h} = -139.5$ km s^{-1}. Direct images of this low surface brightness (LSB) galaxy were obtained with the 6-m telescope of the Special Astrophysical Observatory (SAO) of the Russian Academy of Sciences (Karachentsev et al. 2001) and with the *Hubble Space Telescope* (*HST*). Its colour–magnitude diagram (CMD) shows a red giant branch population and a trace of blue stars. Karachentsev et al. (2001) classify the object as a transition-type galaxy (dIrr/dSph) at the distance of 1.86 Mpc.

On the other hand, the spectral survey of nearby dwarf LSB galaxies with the Russian 6-m telescope failed to detect an optical velocity of KKR 25 (Makarov, Karachentsev & Burenkov 2003). Moreover, deep radio observations with the Giant Metrewave Radio Telescope (GMRT; Begum & Chengalur 2005) did not show significant H I emission in the range $-256 < V_\mathrm{h} < -45$ km s^{-1} at the level $M_\mathrm{H\,I} = 0.8 \times 10^5$ M$_\odot$. Begum & Chengalur (2005) concluded that 'the non-detection of H I in KKR 25 suggests that previous single-dish measurements were affected by confusion with the Galactic emission. Our stringent limits on the H I mass of KKR 25 indicate that it is a normal dSph galaxy'.

KKR 25 is one of the most isolated galaxies inside the sphere of 3 Mpc around us. It settles at the distance of 1.9 Mpc from the Milky Way (MW) and at 1.2 Mpc above the supergalactic plane in the front of the Local Void. KKR 25 is far away from the zero-velocity surface of $R_0 = 0.96 \pm 0.03$ Mpc (Karachentsev et al. 2009), which separates the Local Group from the cosmic expansion. The Local Group is the nearest massive structure to KKR 25. The second close massive group is the M 81 at the distance of 2.56 Mpc.

★E-mail: dim@sao.ru
†Deceased.

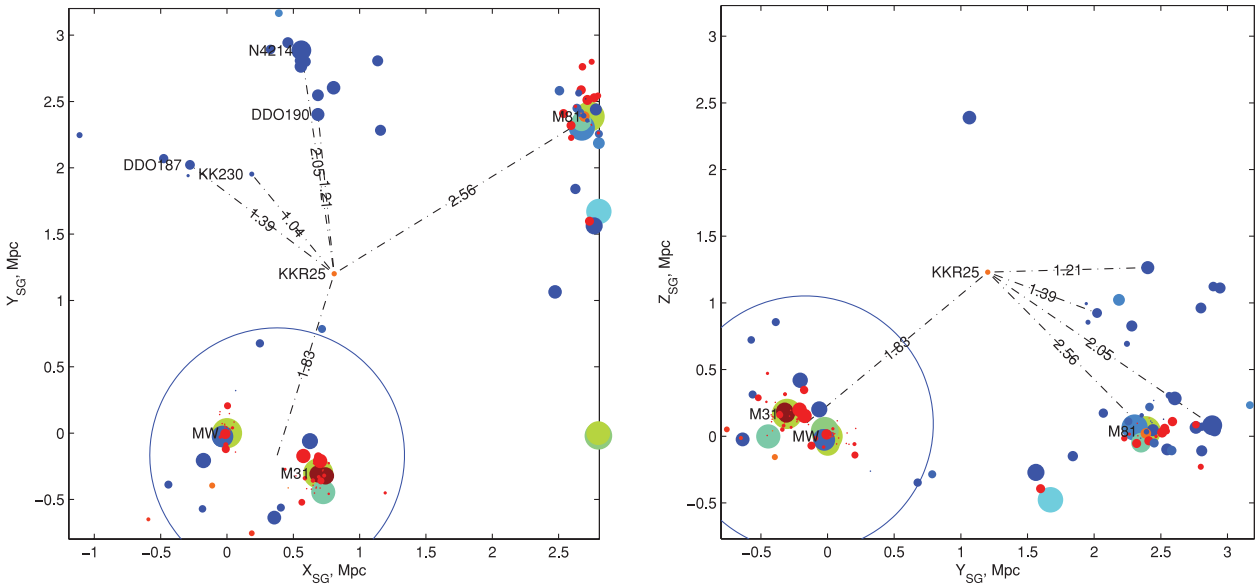

Figure 1. The map of galaxies in the supergalactic coordinates is centred on KKR 25. The left-hand panel presents the projection of galaxies on the supergalactic plane, while the right-hand panel shows the edge-on view on the 'pancake' of galaxies. The filled circle size is proportional to the absolute magnitude of galaxies. Galaxies are coded by a colour from red for early types ($T = -5$) to blue for late types ($T = 10$), according to a morphological type in the de Vaucouleurs numerical scale (de Vaucouleurs et al. 1991). The zero-velocity surface is shown by a big blue circle around the Local Group. Distance to the nearby structure is marked by dash–dotted lines with the corresponding distance written on it. The brightest galaxies in the volume under consideration are the Milky Way (MW), Andromeda galaxy (M31) and M81. They are signed on the figures. KK 230 is the closest galaxy to KKR 25. Three associations of dwarf galaxies (Tully et al. 2006) are shown in the left-hand panel. DDO 190 is the brightest member of 14+08 association. DDO 187 corresponds to 'Dregs' association and NGC 4214 to 14+07. The Local Void occupies the upper half of the right-hand panel just above KKR 25.

There are no galaxies closer than 1 Mpc to KKR 25 (see Fig. 1). The nearest neighbour is the dwarf galaxy KK 230 ($M_B = -9.8$). The isolation of KKR 25 was pointed out by Karachentsev et al. (2001). Tully et al. (2006) note that KKR 25 is the only isolated galaxy on the scale of 3 Mpc from us and 'every object in this volume is associated with either a luminous group, an association of dwarfs or the dregs evaporating association'. Two associations 14+08 (around DDO 190) and 'Dregs' (around DDO 187) stand on the distance of 1.2 and 1.4 Mpc from KKR 25, respectively.

In spite of its isolation KKR 25 has no gas and looks like a normal dSph system. This fact draws our attention because we expect to find dSph galaxies in dense regions, like groups and clusters of galaxies. Obviously, any kind of interaction with a massive galaxy is not suitable to explain the properties of KKR 25. This galaxy can play a crucial role in testing of different scenarios of dSph's formation.

Karachentsev et al. (2001) have found a globular cluster (GC) candidate in the *HST* images of the galaxy. An apparent magnitude of the object $V_T = 20.59$ corresponds to $M_V = -5.79$, which is typical for Galactic GCs. In the framework of the Hα survey of the Canes Venatici I cloud of galaxies with the Russian 6-m telescope, Kaisin & Karachentsev (2008) have also found a faint Hα knot on the northern side of KKR 25. A measured flux of the knot is $\log F = -14.64$ erg cm^{-2} s^{-1}. These interesting objects were targeted for a spectroscopic study with the 6-m telescope in the current study.

The main parameters of KKR 25 are presented in Table 1. The coordinates are taken from HyperLEDA[1] (Paturel et al. 2003). Apparent sizes were published by Karachentseva et al. (1999). The colour $(V - I)_T$ was measured by Karachentsev et al. (2001).

[1] http://leda.univ-lyon1.fr/

Table 1. Main parameters of KKR 25.

RA (J2000)	16 13 47.6	HyperLEDA
Dec. (J2000)	+54 22 16	HyperLEDA
$E(B-V)$ (mag)	0.008	Schlegel, Finkbeiner & Davis (1998)
Size (arcmin)	1.1 × 0.65	Karachentseva et al. (1999)
h (arcsec)	16.7 ± 1.1	This work
b/a	0.51 ± 0.03	This work
V_T (mag)	15.52 ± 0.22	This work
$(V-I)_T$ (mag)	0.88	Karachentsev et al. (2001)
Σ_V (mag/□″)	23.97 ± 0.03	Karachentsev et al. (2001)
V_h(stars) (km s^{-1})	−65 ± 15	This work
V_h(PN) (km s^{-1})	−79 ± 9	This work
$(m-M)_0$ (mag)	26.42 ± 0.07	This work
Distance (Mpc)	1.93 ± 0.07	This work
V_{LG} (km s^{-1})	128	This work
M_V (mag)	−10.93	This work
L_V (×10^6 L$_\odot$)	2.0	This work
Σ_V (L$_\odot$ pc^{-2})	9.6	This work

The central surface brightness Σ_V was estimated from the profiles published by Karachentsev et al. (2001). All other values, total magnitude V_T, axis ratio, scale length h, heliocentric velocity V_h and distance modulus $(m-M)_0$, are derived in the current work. The V_T, $(V-I)_T$ and Σ_V magnitudes are not corrected for Galactic extinction.

2 DIRECT IMAGES

2.1 Observations and photometry

KKR 25 was first observed with the Wide Field Planetary Camera 2 (WFPC2) on 2001 May 28 as a part of the *HST* snapshot project (proposal 8601; PI: P. Seitzer). Two exposures were made

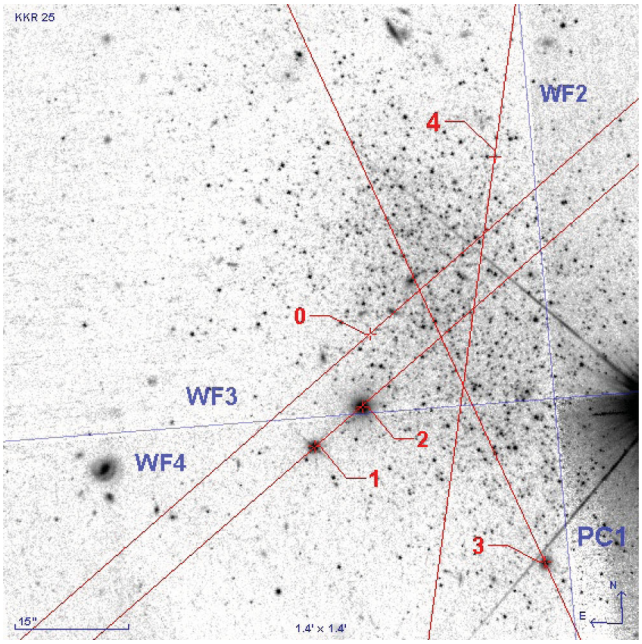

Figure 2. The *HST*/WFPC2 image of KKR 25 in the *F*814*W* band. The bounds of planetary (PC1) and wide field cameras (WF2, WF3, WF4) are shown. The main part of KKR 25 is arranged in the WF3 chip. A bright star fully saturates the PC1 camera. The objects for the spectroscopic study are numbered. The long slit positions are overplotted. The integrated spectrum of the stellar light was obtained in the slit position '0'.

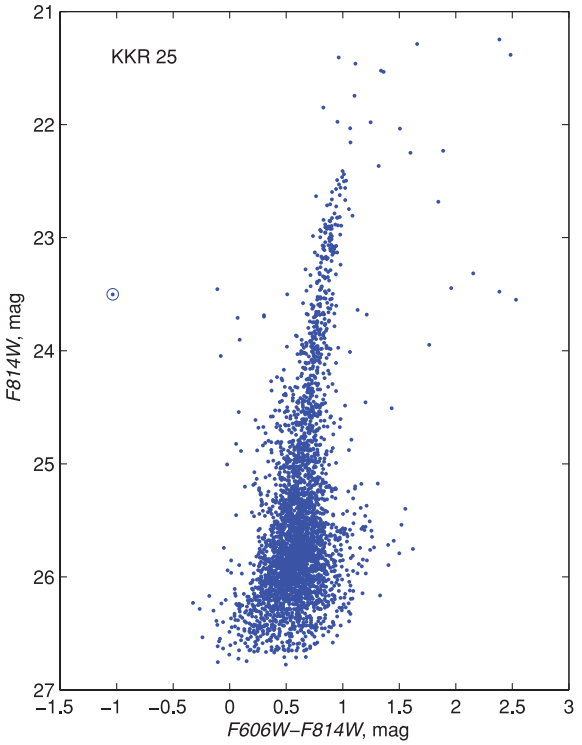

Figure 3. The CMD based on the *HST*/WFPC2 image of KKR 25. Extremely blue object 4 from our spectroscopic study is shown by an open circle.

with filters *F*606*W* (broad-band *V*) and *F*814*W* (broad-band *I*). The exposure time is 600 s in each filter. Later, the galaxy was observed with WFPC2 on 2009 March 23–25 within the ACS Nearby Galaxy Survey Treasury (ANGST) project (Dalcanton et al. 2009). Deep exposures in *F*606*W* (4800 s) and *F*814*W* (9600 s) were made. The image of KKR 25 is shown in Fig. 2. Stellar photometry procedures, artificial star experiments and star formation history (SFH) measurements were made for both the exposure sets. The results of the SFH measurements are in good agreement. We have decided to consider only the deeper exposure data in this paper. All descriptions below are related to the project 11986 (PI: J. Dalcanton) *HST*/WFPC2 images. The WFPC2 images were obtained from the Space Telescope Science Institute (STScI) archive using the standard processing and calibration pipeline. A photometry of resolved stars in the galaxy was made with the HSTPHOT package (Dolphin 2000), following procedures and recipes indicated in the HSTPHOT Users Guide.[2] The data quality images were used to mask bad pixels. Cosmic rays were masked using the HSTPHOT *crmask* utility. Only stars with photometry of good quality [signal-to-noise ratio (S/N) $\geq$5 in both filters, $|\chi| < 2.5$, |sharp| < 0.3 and type ≤ 2] were used in the analysis. The resulting CMD is presented in Fig. 3.

Artificial star tests were performed using the same reduction procedures to estimate photometric errors correctly. We have created a large library of artificial stars distributed in the same range of stellar magnitudes and colours as the original measured stars. Spatial distribution of the artificial stars was also resembling the original one so that the recovered photometry is adequately sampled. The photometric errors and completeness are represented in Fig. 4.

[2] http://purcell.as.arizona.edu/hstphot/hstphot.ps.gz

2.2 Reddening and background contamination

KKR 25 is situated at a rather high Galactic latitude and the Galactic extinction is not large for this galaxy: $A_V = 0.028$ and $A_I = 0.016$ mag according to Schlegel et al. (1998). As can be seen from the CMD of KKR 25, the field is not heavily contaminated by background stars. In order to estimate a number of foreground/background stars in the CMD, we have used TRILEGAL (Girardi et al. 2005) to simulate star counts in our Galaxy. TRILEGAL simulates CMDs in the WFPC2 instrumental system taking into account the components of thin and thick Galactic discs, the halo and the bulge of our Galaxy. The photometric errors, the saturation and the incompleteness were taken into account in the modelling. These models confirm a negligible contamination by foreground stars. An expected number of foreground stars in the CMD is about 43 ± 6 up to the photometric limit $I = 27.0$ mag.

2.3 Distance determination

A photometric distance to KKR 25 was first estimated by Karachentsev et al. (2001) using a tip of the red giant branch (TRGB) distance indicator. They have obtained a true distance modulus of $(m - M)_0 = 26.35 \pm 0.14$ mag and a respective distance of $D = 1.86 \pm 0.12$ Mpc. TRGB distances for several galaxies in M 81 group were recently measured also by Dalcanton et al. (2009) within their ANGST project. However, the older data set was used for their KKR 25 distance measurement in this paper. They determined a distance modulus of KKR 25 as $(m - M)_0 = 26.43$.

The recent deep *HST*/WFPC2 observations and accurate HSTPHOT photometry allow us to estimate a TRGB distance with better uncertainties. The TRGB method was also considerably improved recently. We have determined a photometric TRGB distance with

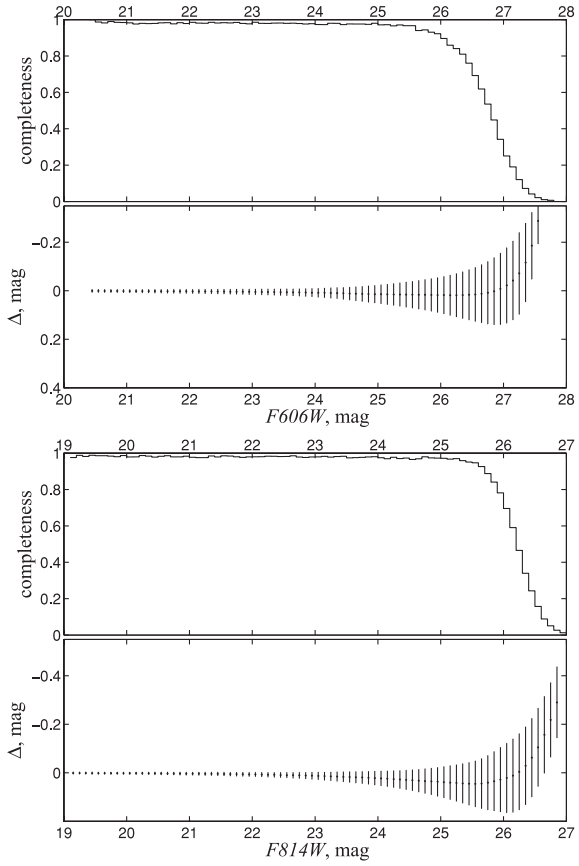

Figure 4. Photometric errors and completeness of KKR 25 in the ANGST project. The photometry statistics were obtained using artificial star tests. The input, 'true' magnitude of artificial stars in $F606W$ and $F814W$ filters are shown on the abscissa. The completeness panel represents a fraction of detected artificial stars as a function of input magnitude. The dispersion and bias of difference between 'observed' and 'true' magnitudes ($\Delta = m_{\rm obs} - m_{\rm true}$) are shown on bottom panels for both passbands.

our TRGBTOOL program, which uses a maximum likelihood algorithm to determine the magnitude of TRGB from the stellar luminosity function (Makarov et al. 2006). The estimated value of TRGB is $F814W = 22.41 \pm 0.07$ mag in the WFPC2 instrumental system. The uncertainty of the TRGB value estimation is dominated by poor statistics in the considered region of the CMD. The calibration of the TRGB distance indicator was recently improved (Rizzi et al. 2007). Colour dependence of an absolute magnitude of TRGB and zero-point issues in *HST*/Advanced Camera for Surveys (ACS) and WFPC2 were addressed in the paper. Using this calibration, we have obtained the true distance modulus for KKR 25 as $(m - M)_0 = 26.42 \pm 0.07$ mag and the respective distance as $D = 1.93 \pm 0.07$ Mpc. Both internal and calibration errors were taken into account in the error budget. The precision of the Galactic extinction value (16 per cent on the Schlegel's maps) was also accounted. The new value is in good agreement with all the previous distance measurements.

2.4 Star formation history

The CMD of KKR 25 (see Fig. 3) shows very tight and clean red giant branch, in the lower part of which, near the photometric limit ($F814W \sim 25.5$–26.5), we can see signs of a red clump. Judging from the CMD, we can expect low abundance and low age spread for the oldest stars in the galaxy. The extremely blue object in the CMD was classified by us as a planetary nebula (PN) belonging to KKR 25. The spectroscopic study of the PN is given below.

First, a star formation rate (SFR) dependence from an age for KKR 25 was measured by Weisz et al. (2011) within their sample of 60 nearby galaxies. We determined detailed SFH of KKR 25 from its CMD using our STARPROBE package (Makarov & Makarova 2004). This program fits the observed photometric distribution of stars in the CMD to a positive linear combination of synthetic diagrams of single stellar populations (SSPs, single age and single metallicity). The algorithm and package are described in detail in the paper of Makarov & Makarova (2004), and the package application to SFH determination for some nearby galaxies is described in our work (Makarova et al. 2010). The observed data were binned into Hess diagram, giving number of stars in cells of the CMD. The size of the cells is 0.05 mag in luminosity and colour. The colour and magnitude limits of the constructed Hess diagram are $-0.3 < F606W - F814W < 2.5$ and $21.0 < F814W < 26.8$. Synthetic Hess diagrams were constructed from theoretical stellar isochrones and initial mass function (IMF). We used the Padova2000 set of theoretical isochrones (Girardi et al. 2000) and a Salpeter (1955) IMF. We create a grid of the isochrones interpolated by age to fill gaps between the original isochrones. The original metallicity set was not altered. The distance was taken from the present paper (see above) and the Galactic extinction is from Schlegel et al. (1998). A binary fraction was assumed to be 30 per cent. The mass function of individual stars and the main component of a binary system are supposed to be the same. The mass distribution for the second component was taken to be flat in the range 0.7–1.0 of the main component mass.

The synthetic diagrams were altered by the same incompleteness and crowding effects, and photometric systematics as those determined for the observations using artificial star experiments. The synthetic diagrams cover all the range of ages (from 0 Myr to 13.7 Gyr) and metallicities (from $Z = 0.0001$ to 0.03). The best-fitting combination of synthetic CMDs is a maximum likelihood solution taking into account the Poisson noise of star counts in the cells of Hess diagram. The resulting SFH is shown in Fig. 5. The 1σ error of each SSP is derived from an analysis of the likelihood function.

The SFHs from our work and Weisz et al. (2011) are in general good agreement. The main difference is in the duration of star formation episodes. Weisz et al. (2011) used six fixed periods of

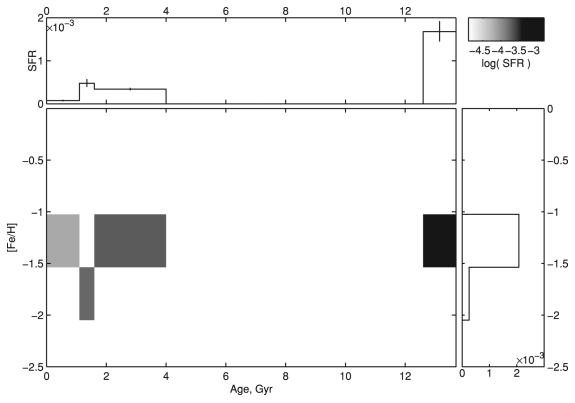

Figure 5. The SFH of the dwarf galaxy KKR 25. The top panel shows the SFR ($M_\odot\ yr^{-1}$) against the age of the stellar populations. The bottom panel represents the metallicity of stellar content as a function of age. The grey-scale colour corresponds to the strength of SFR for the given age and metallicity.

star formation for all 60 galaxies, while in our measurement we have a sophisticated algorithm of star formation periods fitting. First, we divided the galaxy lifetime into quite small steps (0.5 Gyr between 0 and 2 Gyr and 2 Gyr between 2 and 13.7 Gyr). In the resulting SFH, we selected five episodes of star formation with constant SFR. A variation of bounds between these episodes of star formation allows us to determine the best fitting of the models to the CMD.

According to our measurements, a main star formation event in KKR 25 has occurred 12.6–13.7 Gyr ago with a mean SFR of $1.7 \pm 0.2 \times 10^{-3}$ $M_\odot$ yr^{-1}. It is the total SFR over the whole galaxy. A metallicity range for the stars formed during this event is about [Fe/H] = [−1.6: −1] dex. This initial burst accounts for 62 per cent of the total mass of formed stars.

A quiescence period appeared about 4–12.6 Gyr ago. There are indications of intermediate-age star formation in KKR 25 between 1 and 4 Gyr with no significant signs of metal enrichment for these stars. The SFR is lower in this period and is equal to 3.6×10^{-4} $M_\odot$ yr^{-1}. The measured SFR is very low for the recent 1 Gyr in this dwarf galaxy: $0.7 \pm 0.3 \times 10^{-4}$ $M_\odot$ yr^{-1}. We found the total mass of the formed stars during KKR 25 lifetime to be $3.0 \pm 0.3 \times 10^6$ $M_\odot$.

3 STRUCTURE OF THE GALAXY

Total and surface photometry of KKR 25 are difficult tasks because of a bright foreground star at 20 arcsec from the centre of the galaxy. However, the HSTPHOT stellar photometry is reliable and is much less affected by a bright star. Moreover, this influence can be taken into account quantitatively.

We used the stellar photometry of the deep WFPC2 images to study a distribution of the stars in the galaxy. Our approach is based on the maximum likelihood fit that was described by Martin, de Jong & Rix (2008). The likelihood function of stellar distribution in the focal plane is defined as

$$\mathcal{L} = \prod_i^N l_i(p_1, p_2, \ldots, p_k), \quad (1)$$

where $l_i(p_1, p_2, \ldots, p_k)$ is the probability of finding a star i given by the set of parameters $p_1, p_2, \ldots, p_k$ with the total number of stars N. This probability is determined by the surface density distribution of foreground and galactic stars, as well as the photometric completeness. Since KKR 25 is located at the high Galactic latitude ($b = +44.4$) and the contamination of CMD by foreground stars is very insignificant, we can neglect the contribution of foreground objects. For the analysis we have selected only stars with $F814W < 26$, which corresponds to the completeness level of about 80 per cent. We have tested the behaviour of completeness over the field of view. We did not find valuable variations in the body of the galaxy except for regions near the brightest foreground stars. For instance, the bright foreground star affects the PC1 and partially WF2 cameras, which is seen in Fig. 2. We excluded these regions from consideration. Distribution of stars in the areas under consideration is shown in Fig. 6. The probability can be expressed in the form

$$l_i(p_1, p_2, \ldots, p_k) = \Sigma(x_i, y_i | p_1, p_2, \ldots, p_k), \quad (2)$$

$$N = \iint_D \Sigma(x, y | p_1, p_2, \ldots, p_k)\, \mathrm{d}x\, \mathrm{d}y, \quad (3)$$

where Σ is the model of surface density distribution with k parameters $p_1, p_2, \ldots, p_k$ and D is the consideration domain.

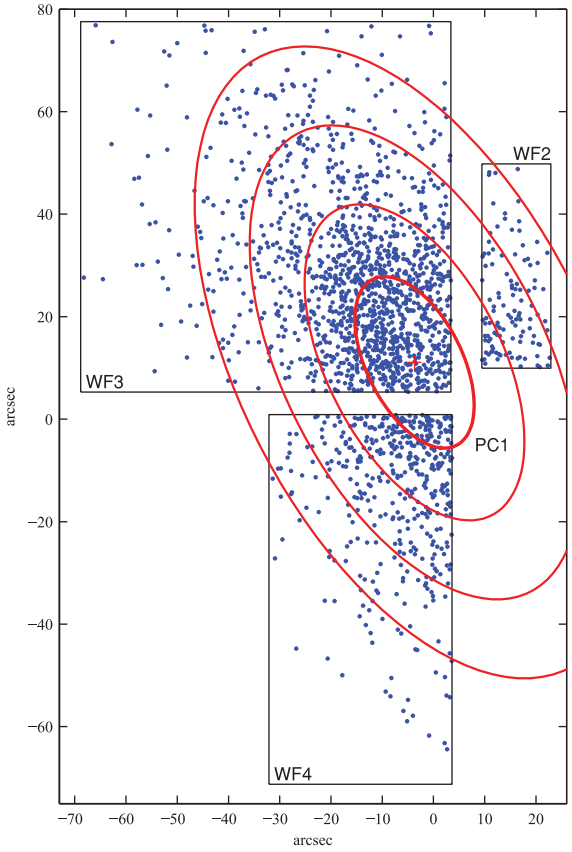

Figure 6. Distribution of the selected stars ($F814W < 26$) of KKR 25 in the frame of WFPC2. The boxes represent the considered areas of the cameras WF2, WF3 and WF4. The PC1 camera was affected by a bright star and was not included in the analysis. The thick ellipse shows the size of the central region of constant stellar density. The set of thin ellipses corresponds to two, three and four times of the exponential scale length. The cross indicates the centre of the galaxy.

We tested a set of models of surface density distribution: the exponential, exponential with central depression, King (1962), Plummer (1911) and Sérsic (1968) profiles.

The WFPC2 coordinates of 1859 selected stars were corrected for the distortion and were transformed to the reference chip using *metric* procedure from STSDAS.HST_CALIB.WFPC package. For each model we derived a centre, position angle and axes ratio of the galaxy (four parameters) as well as scale length parameters of the model (from one to three parameters). The central surface density is derived as normalization coefficient to the total number of stars.

We used the Akaike Information Criterion AIC $= -2 \ln \mathcal{L} + 2k$ (Akaike 1974) and the Bayesian Information Criterion BIC $= -2 \ln \mathcal{L} + k \ln N$ (Schwarz 1978), where N is the sample size, i.e. the number of selected stars in our case. These criteria regulate the balance between the improvement of model by additional parameters and the number of parameters needed to achieve this improvement. One should prefer a model with a minimal value of the criterion. An absolute value of the criterion is not informative, while the difference between the AIC or BIC values for two fits provides an estimate of evidence for one model against another. The BIC difference $0 < \Delta_{BIC} < 2$ is not worth more than a bare mention, $2 < \Delta_{BIC} < 6$ represents positive evidence, $6 < \Delta_{BIC} < 10$ means strong evidence and $\Delta_{BIC} > 10$ means very strong evidence (Kass & Raftery 1995). There are similar guidelines for Δ_{AIC} values

Table 2. A comparison of the different models of stellar population distribution of KKR 25. Δ_{AIC} and Δ_{BIC} are computed, respectively, to the model with a minimal value of the criterion.

Model	k	$\ln \mathcal{L}$	Δ_{AIC}	Δ_{BIC}
exp	5	−9963.4	43.6	38.1
exp 1	6	−9940.6	0.0	0.0
exp 2	7	−9940.3	1.5	7.0
Plummer	5	−9956.0	28.9	23.4
Sérsic	6	−9949.2	17.2	17.2
King	6	−9946.4	11.7	11.7

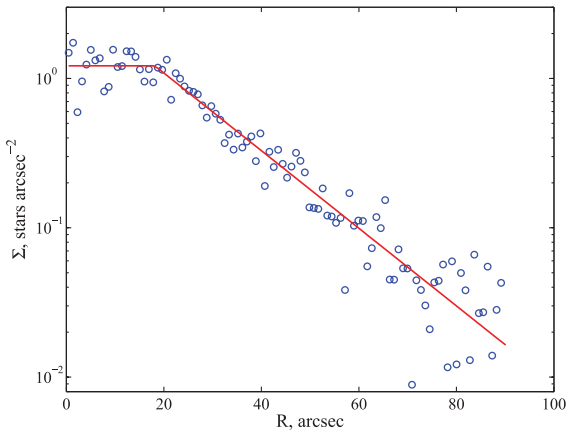

Figure 7. Surface density profile of the selected stars in KKR 25. The stellar density is measured in concentric elliptical annuli from the centre. The solid line represents the best-fitting model, the exponential profile with the depression in the central region. The parameters of the model were determined using the maximum likelihood method.

(Burnham & Anderson 2004). More details on a model selection can be found, for instance, in Liddle (2007).

A comparison of different models is presented in Table 2. The 'exp 1' and 'exp 2' code the models of exponential profile with central depression. These models differ from simple exponent within a specific radius near the centre of the galaxy. The 'exp 1' corresponds to the model with a constant density in the centre, the 'exp 2' is an exponential decay in the central part of the galaxy. Taking into account only likelihood value, we can conclude that the pure exponential profile is the worst case of all. However, the simple modification of the exponential model with depression in the centre improves the fit significantly, and these models leave behind all other models under consideration. The AIC and BIC clearly select exponential profile with the constant surface density in the central region (exp 1) as the best-fitting model for the given distribution of the stars.

Stellar density profile of KKR 25 is shown in Fig. 7. Structural parameters of the best model are summarized in Table 3. The galaxy shows the exponential profile with an axial ratio of 1:2 and a flat distribution of the surface brightness near the centre. The angular size of the central depression roughly equals the exponential scale length. We have estimated an integrated magnitude of the galaxy from the derived model parameters (see Table 3, 'all') and the central surface density $\Sigma_V = 23.97$ and $\Sigma_I = 23.09$ mag, which were taken from our previous photometry results (Karachentsev et al. 2001). We obtained the total magnitudes of KKR 25, i.e. $V_T = 15.52 \pm 0.22$ and $I_T = 14.64 \pm 0.22$. The new V_T value is 0.4 mag brighter than $V_T = 15.9$ obtained by Karachentsev et al. (2001). The difference

Table 3. Parameters of the 'exp 1' model for different star selections. h is an exponential scale length, b/a is an axes ratio of the stellar distribution and R is the central depression radius.

	All $F814W < 26$	RGB $F814W < 25.5$	RC $25.5 < F814W < 26$
h (arcsec)	$16.7^{+1.1}_{-1.0}$	$18.4^{+1.7}_{-1.4}$	$15.7^{+1.4}_{-1.3}$
h (pc)	156^{+12}_{-11}	172^{+17}_{-14}	147^{+14}_{-13}
b/a	$0.51^{+0.03}_{-0.03}$	$0.46^{+0.04}_{-0.04}$	$0.55^{+0.05}_{-0.04}$
R (arcsec)	$18.2^{+2.3}_{-3.1}$	$12.4^{+4.3}_{-6.4}$	$20.5^{+2.8}_{-2.8}$
R (pc)	170^{+22}_{-30}	116^{+40}_{-60}	192^{+27}_{-27}

can be explained by difficulties of photometry caused by the nearby bright star and the small field of view where the galaxy occupies the whole WF3 chip of WFPC2.

There is an indication on a slightly different spatial distribution of red giant branch and red clump stars. These populations are indicated as RGB and RC in Table 3, respectively. Judging from the scale length, the RC population is slightly more centrally concentrated than RGB stars. But the difference appears on the level of 2σ.

4 SPECTROSCOPY

4.1 Observations and data reduction

We have carried out several sets of long-slit observations of a GC candidate, bright objects and Hα source in KKR 25. The spectroscopic data were obtained with the Spectral Camera with Optical Reducer for Photometrical and Interferometrical Observations (SCORPIO)[3] (Afanasiev & Moiseev 2005) in the prime focus of the Russian 6-m telescope.

We used the grism VPHG550G (550 lines mm^{-1}) and 2k × 2k CCD EEV42–40 detector. This combination together with the slit of 6 arcmin × 1 arcsec provides a spectral resolution ∼10 Å in the range of 3500–7200 Å. A typical dispersion was 2.1 Å pixel^{-1}. The frames were binned by 2 pixel along the slit direction, resulting in a spatial scale of 0.357 arcsec pixel^{-1}. For wavelength calibration we used He–Ne–Ar lamp.

The journal of observations is presented in Table 4. Orientations of the slit are shown on the direct WFPC2 image of the galaxy in Fig. 2.

The standard data reduction and analysis were performed using the European Southern Observatory Munich Image Data Analysis System[4] (ESO-MIDAS; Banse et al. 1983) and the Image Reduction and Analysis Facility (IRAF) software.[5] The dispersion solution determines an accuracy of the wavelength calibration ∼0.14 Å. The wavelength zero-point can be shifted up to 2 pixel during the night. This effect was corrected using the night sky lines in the dispersion-corrected spectra. An extraction of the spectra was made using the IRAF procedure *apsum*. After the wavelength calibration and sky subtraction, the spectra were corrected for atmospheric extinction and flux-calibrated using the observed spectrophotometric standard stars (Oke 1990). Finally, all one-dimensional spectra of each object were summed to increase the S/N. We observed bright radial velocity standard stars (Barbier-Brossat & Figon 2000) at the end of

[3] http://www.sao.ru/hq/lsfvo/devices/scorpio/scorpio.html
[4] http://www.eso.org/sci/software/esomidas/
[5] http://iraf.noao.edu/

Table 4. The journal of spectroscopic observations.

Object	Date	Exposure (s)	Seeing (arcsec)
KKR 25 slit pos. 1–2	08/02/05	900 × 2	2.0
KKR 25 slit pos. 3	09/02/05	900 × 3	1.6
KKR 25 slit pos. 0	10/02/05	1200 × 3, 900	2.5
KKR 25 slit pos. 4	30/05/09	1200 × 3, 900	2.3
KKR 25	07/08/11	1200 × 3	1.5
Radial velocity standard stars			
BD +23 992	08/02/05	10	2.0
	09/02/05	10 × 2	2.0
	10/02/05	10 × 2	2.5
BD +23 680	08/02/05	10 × 2	2.0
BD +23 655	09/02/05	30 × 2	2.0
BD +23 751	10/02/05	10 × 2	2.5
BD +23 708	10/02/05	20	2.5
Spectroscopic standard stars			
SA 95–42	08/02/05	60	2.0
BD +75 325	09/02/05	30 × 2	2.0
	10/02/05	30 × 2	2.2
BD +33 2642	30/05/09	60	2.6
LDS 749 B	07/08/11	30 × 2	1.5

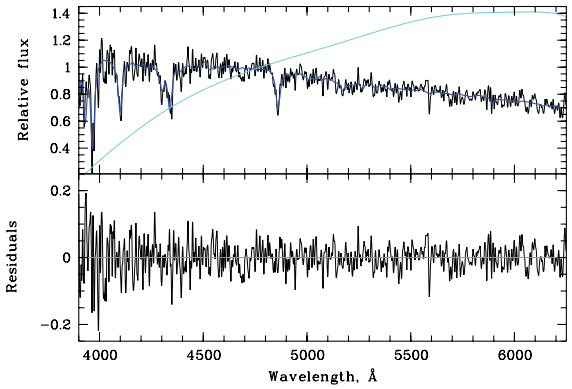

Figure 8. Top: integrated spectrum of the stellar light of KKR 25 (black) in comparison with a composite model (dark blue). The fitting is produced with the Vazdekis et al. (2010) SSP model and the Miles stellar library. The result of the division of the normalized model and object spectra is demonstrated in light blue. Bottom: the difference between the normalized object and model spectra. The zero line is green.

each night to obtain heliocentric radial velocities of the programme objects using the method of Tonry & Davis (1979), and to obtain the line spread function (LSF) of the spectrograph.

4.2 Integrated stellar light of KKR 25

The spectra of integrated light of the KKR 25 were obtained during the observations on 2005 February 10 (Table 4). We combined these spectra with the data received in 2009 and 2011. The S/N per wavelength measured in the total integrated light spectrum at $\lambda \sim 5500$ Å is 54, at $\lambda \sim 4000$ Å is 15, and goes down at $\lambda \geq 5577$ Å due to the bright emission sky lines. The resulting spectrum is demonstrated in black in Fig. 8 (top).

The STECKMAP program (Ocvirk et al. 2006a,b) with the PEGASE.HR model grids (Le Borgne et al. 2004) and the ULYSS[6] program with the PEGASE.HR model grid and the Elodie (Prugniel & Soubiran 2001) and Miles (Sánchez-Blázquez et al. 2006) stellar libraries,[7] and the Vazdekis (Vazdekis et al. 2010) SSP model with the Miles stellar library were employed to analyse stellar populations in KKR 25. We use Salpeter (1955) IMF in all these cases. Comparison of the fitting results for the three sets of models allows us to claim that ∼70–100 per cent of the light fraction in KKR 25 is as old as 2–14 Gyr and has a low mean metallicity [Fe/H] $\sim -1.75 \pm 0.15$ dex. Unfortunately, because of the low surface brightness of KKR 25 the night sky lines affect the resulting spectrum, especially in the red part. Thus, we cannot reliably estimate the contribution and properties of the second stellar component with an age of 1–2 Gyr.

One of the three fittings is illustrated in Fig. 8, where a two-component model (the Vazdekis et al. 2010 SSP model with the Miles stellar library) is shown in dark blue. This model is completely composed of old metal-poor (age ∼ 18 Gyr, [Fe/H] = −1.68 dex) population. The difference between the normalized object and model spectra (Fig. 8, bottom) is less than or equal to 10 per cent. Broad absorption-line features are noticeable near 4227, 4455, ∼4700, 5036 and ∼5200 which were not fitted well by the models. They may be composed of TiO, Ca I, Mn I and Mg I lines. The relative intensity of such lines may indicate substantial α element enhancement, and the presence of dust in the interstellar medium blown out by previous generations of asymptotic giant branch stars (Boyer 2008). The obtained [Fe/H] is in good agreement with the stellar population CMD study presented in Section 2.4. We determined that the radial velocity of the stellar component in KKR 25 is $V_h = -65 \pm 15$ km s^{-1}.

Table 5. List of spectroscopically observed objects. The columns are (1) object number in Fig. 2; (2) equatorial J2000 coordinates; (3, 4) V-band magnitude and $V - I$ colour (HSTPHOT in the case of PN and aperture photometry in all other cases); (5) heliocentric radial velocity in km s^{-1}; (6) classification.

N	RA (2000) Dec.	V	$V - I$	V_h	Note
1	161350.0+542201	21.6 ± 0.13	3.2 ± 0.10	-350 ± 52	Star
2	161349.3+542206	20.5 ± 0.12	1.7 ± 0.10	100431:	S0
3	161346.5+542145	21.3 ± 0.15	1.0 ± 0.25	224844:	quasar
4	161347.2+542239	22.11 ± 0.11	-1.54 ± 0.14	-79 ± 9	PN

4.3 Bright objects in the field of KKR 25

The diffuse GC candidates (2, 3) and a very red star (1) were selected for spectroscopic survey using the snapshot *HST* images (see Fig. 2). Spectra of these objects were obtained with the 6-m telescope in 2005 (Table 4) in the framework of the project 'Searches for GCs in nearby dwarf galaxies' (PI: T. H. Puzia). The targets are indicated by numbers in Fig. 2. The candidate found by Karachentsev et al. (2001) has number 2 in our list. The results of the survey are summarized in Table 5.

The spectra of GC candidates are shown in Fig. 9. We compared them with the templates of Kinney et al. (1996). The object selected by Karachentsev et al. (2001) appears to be an S0 galaxy with redshift $z \sim 0.335$. Another bright target is a quasar at $z \sim 0.75$.

The spectrum of the object 1 revealed the nature of this star as an M-type dwarf (see Fig. 10). Therefore, it does not belong to KKR 25.

As a result of our survey, we did not confirm the presence of GCs in KKR 25.

[6] http://ulyss.univ-lyon1.fr

[7] http://ulyss.univ-lyon1.fr/models.html

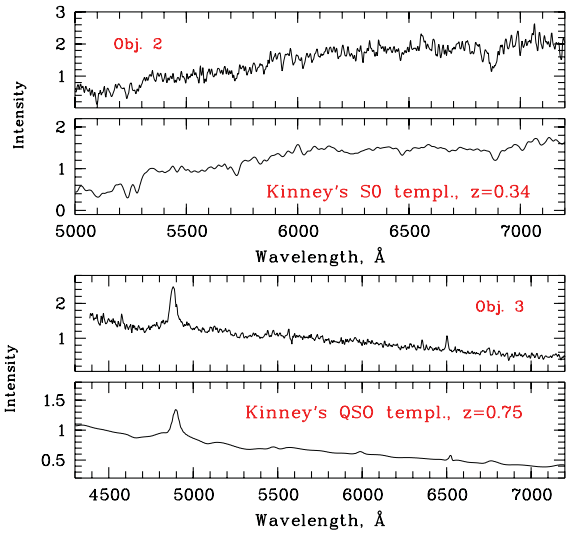

Figure 9. Spectra of background objects (2 and 3, Fig. 2) obtained at the 6-m telescope. Kinney et al. (1996) templates are shown for comparison.

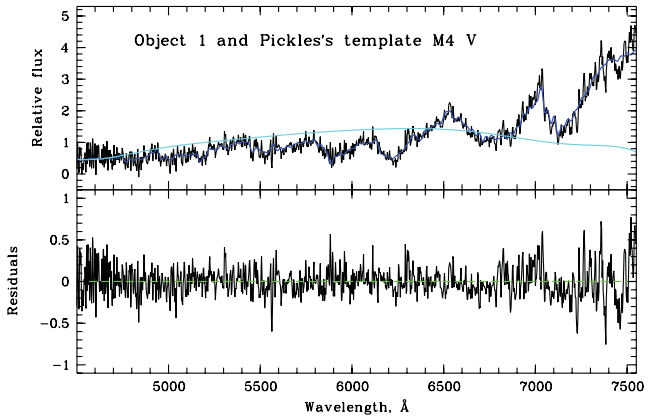

Figure 10. Spectrum of a bright red star near KKR 25. The top panel shows the observations (black) in comparison with the normalized template (Pickles 1998) of M4V star (dark blue). The light-blue line demonstrates a multiplicative term applied to the original spectrum to bring it into the correspondence to the stellar template. The lower panel shows the fitting residuals.

4.4 Hα object

A faint Hα emission at the northern side of KKR 25 was discovered by Kaisin & Karachentsev (2008) in their Hα survey of galaxies in the Canes Venatici I cloud. However, the WFPC2 image does not show any extended object in the corresponding area of the galaxy. We identified an Hα object with unusual extremely blue star which is indicated with number 4 in the direct image (Fig. 2) and with a circle in the CMD (Fig. 3).

Taking into account that HSTPHOT perfectly fits this object with stellar profile (sharp = −0.001), and assuming that the object belongs to the galaxy, we can estimate an upper limit on the linear size of Hα source. Because the object profile is not wider than point spread function (PSF), we could assume that its angular size is smaller than the full width at half-maximum (FWHM) for a stellar profile. Thus, Hα source diameter should be less than 1.9 pc for WFPC2's FWHM ∼ 0.2 arcsec at the distance of 1.93 Mpc. The median radius of old PNe is ∼0.6 pc, while young PNe typically have radii <0.05 pc (Frew & Parker 2010). Although, H II regions have sizes from tens to hundreds of parsecs (Oey et al. 2003), the ultra-

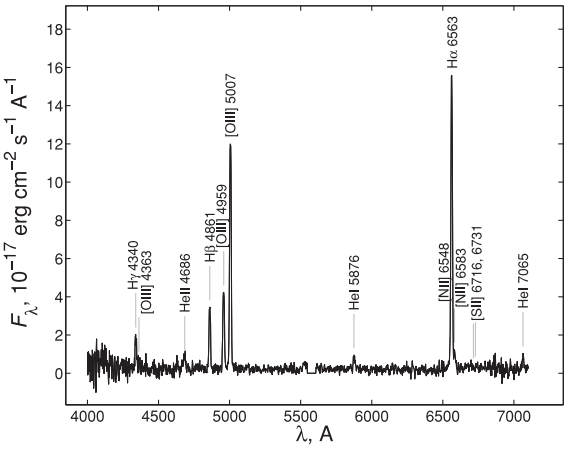

Figure 11. The spectrum of the Hα object.

Table 6. Line intensities of the Hα object.

Ion	λ (Å)	$F(\lambda)/F(\mathrm{H}\beta)$	$I(\lambda)/I(\mathrm{H}\beta)$
Hγ	4340.47	0.52 ± 0.08	0.66 ± 0.13
[O III]	4363.21	0.07 ± 0.05	0.08 ± 0.07
He II	4685.70	0.30 ± 0.07	0.32 ± 0.08
Hβ	4861.33	1.00 ± 0.08	1.00 ± 0.10
[O III]	4958.92	1.36 ± 0.10	1.30 ± 0.10
[O III]	5006.85	4.07 ± 0.26	3.82 ± 0.25
He I	5875.60	0.23 ± 0.05	0.16 ± 0.04
N II	6548.10	0.08 ± 0.04	0.04 ± 0.02
Hα	6562.80	5.05 ± 0.30	2.80 ± 0.19
N II	6583.40	0.26 ± 0.06	0.14 ± 0.03
He I	7065.30	0.25 ± 0.05	0.12 ± 0.03

compact H II regions have diameters <0.1 pc (Wood & Churchwell 1989), i.e. comparable in size with PNe.

Thus, an intriguing question is the nature of the Hα emission in KKR 25. We carried out two sets of spectroscopic observations of the Hα object with the 6-m telescope on 2009 May 30 and 2011 August 8 (see Table 4). Each of the three exposures of 1200 s was obtained along the parallactic angle to minimize the influence of the atmospheric refraction. The resulting spectrum is shown in Fig. 11. Besides bright hydrogen and oxygen emissions, we clearly see helium (He I 5876, 7065 and He II 4686) and nitrogen ([N II] 6548, 6583) lines. Table 6 presents measurements of the emission line intensities $F(\lambda)$ relative to Hβ, and the ratios corrected for Galactic and internal extinction $[I(\lambda)/I(\mathrm{H}\beta)]$.

Because the object under consideration is a point-like source, we cannot use morphological properties for classification. Moreover, PN and H II spectra have the same emission lines. The difference is only in intensity ratios due to different temperatures of central source. A central star in a PN is hotter than OB stars in H II regions. Kniazev, Pustilnik & Zucker (2008a) proposed to use the following characteristic diagrams for the separation of PN and H II regions (see formulas 1 and 3 from the original publication):

$$\log \frac{[\mathrm{O\,III}]\,5007}{\mathrm{H}\beta} \geq \left(0.61/\log \frac{[\mathrm{N\,II}]\,6584}{\mathrm{H}\alpha} - 0.47\right) + 1.19, \qquad (4)$$

$$\log \frac{[\mathrm{S\,II}]\,6731, 6717}{\mathrm{H}\alpha} \leq 0.63 \log \frac{[\mathrm{N\,II}]\,6584}{\mathrm{H}\alpha} - 0.55. \qquad (5)$$

These criteria allow us to segregate 99 per cent of the PNe from compact H II regions if an object satisfies to at least one of these

inequalities. According to line intensity measurements (see Table 6), the Hα object passes both criteria. The criterion (4) is satisfied at a level of 12σ. Because sulphur lines [S II] 6731, 6717 were not detected, we used 3σ upper limit for classification. $I([\mathrm{S\,II}])/I(\mathrm{H}\beta) < 0.06$ meets the criterion (5) at least on 4σ level. Thus, we can argue with high reliability that the Hα object is a PN.

Using Hα flux $\log F = -14.64$ erg cm^{-2} s^{-1} from Kaisin & Karachentsev (2008) and the ratio $F([\mathrm{O\,III}])/F(\mathrm{H}\alpha)$ from our measurements (Table 6), we can estimate visible $m_{5007} = -2.5 \log F - 13.74 = 23.09$ (Jacoby 1989), which corresponds to $M_{5007} = -3.35$ for a distance $(m - M)_0 = 26.42$ and $E(B - V) = 0.008$. Note that the estimated absolute magnitude is close to the bright cut-off of the PN luminosity function.

We serendipitously discovered a PN in KKR 25. PNe are not rare in giant galaxies. The PN luminosity function is one of the popular methods for distance determination in the nearby Universe. There are a number of irregular galaxies with known PNe as well as bright dwarf ellipticals NGC 185, NGC 205 near M 31. Till date there are only four dSph systems owning PN. NGC 147 (Gonçalves et al. 2007) is a satellite of M31, and Fornax (Kniazev et al. 2007), Sagittarius dSph (Kniazev et al. 2008b) and transitional-type Phoenix (Saviane et al. 2009) are the satellites of MW. Most of these galaxies are significantly brighter than KKR 25 and contain substantially bigger stellar mass. Only Sagittarius dSph and Phoenix are more or less comparable with KKR 25 by morphology and luminosity. We have found first PN in the dSph galaxy outside the Local Group. An analysis of CMD on existence of extraordinary blue stars gives a fast and easy method for the selection of PN candidates in nearby galaxies.

We have estimated an oxygen abundance of PN to be $12 + \log(\mathrm{O/H}) = 7.60 \pm 0.07$, using the semi-empirical method of Izotov & Thuan (2007). The line [O II] 3727 is invisible on our data. Thus, we estimated it as 2σ of noise in the corresponding part of the spectrum. This contribution to the total abundance of oxygen is negligible, and the variations of its intensity in the range $\pm 1\sigma$ do not change the result.

The PN also allows us to measure the velocity of the galaxy with high precision, which is really challenging for the low surface brightness dSph galaxy without gas. We have estimated the heliocentric velocity of the Hα object, $V_\mathrm{h} = -79 \pm 9$ km s^{-1}, using weighted mean of redshifts of emission lines (Hα, Hβ and [O III] 4959, 5007) in each of the six spectra obtained in 2009 and 2011 with the Russian 6-m telescope.

We have obtained spectra of Hα spot in KKR 25 with the Deep Extragalactic Imaging Multi-Object Spectrograph (DEIMOS) spectrograph on the Keck II 10-m telescope. The observations were carried out during two nights on 2009 February 22 and 23. We received 2 × 5 min spectra on the first night and 3 × 5 min spectra on the second night. The spectroscopic set-up for the DEIMOS observations used the 1200 lines mm^{-1} grating with a central wavelength of 5800 Å. This provides a spectral coverage over a range of 4400–7100 Å, with a dispersion of about 0.33 Å pixel^{-1}. The observations took place against a very bright dawn sky. Nevertheless, each 5 min spectral exposure shows a bright emission line close to Hα position. A weak N II 6548 line is also visible. There is only a hint on N II 6548. We have estimated the heliocentric velocity $V_\mathrm{h} = -54 \pm 12$ km s^{-1} using a combined spectrum.

5 DISCUSSION

We gathered the properties of KKR 25, the Local Group spheroidals outside the virialized zones of the MW and M 31, and highly isolated dIrr KKH 98 in Table 7. The columns contain the galaxy identification; its morphological type; distance in Mpc from the MW, the Andromeda galaxy (M 31) and the centroid of the Local Group (LG); tidal index (TI) and the main disturber as defined by Karachentsev et al. (2004); absolute magnitude M_V; central surface brightness Σ_V corrected for Galactic absorption; metallicity [Fe/H]; total mass M; and mass-to-light ratio M/L_V. The original values were corrected for adopted distance if necessary. The tidal index characterizes in logarithmic scale the tidal influence from the most important nearby galaxy. The negative value corresponds to an isolated object. KKR 25 is 2.5–3 times brighter than Phoenix, Tucana and And XVIII, and is 1.5 times fainter than Cetus – the brightest isolated spheroidal. KKR 25 has the highest surface brightness of all the spheroidal galaxies in our sample.

KKR 25 is very similar to remote dSph galaxies in the Local Group. Cetus, Tucana and And XVIII are the only dSphs which are not definitely satellites of the MW or the Andromeda galaxy. All these galaxies are gas deficient. Any previous H I detections were disproved by direct observations of stellar kinematics of Cetus (Lewis et al. 2007) and Tucana (Fraternali et al. 2009), or by deep radio interferometric observations of KKR 25 (Begum & Chengalur 2005). Only in Phoenix, Gallart et al. (2001) concluded that an H I cloud was associated with the galaxy, but it has been lost after the last star formation episode. KKR 25 resides near the brightest end

Table 7. Properties of nearby isolated galaxies.

Galaxy	Type	MW M 31 LG (Mpc)	TI	MD	M_V (mag)	Σ_V (mag)	[Fe/H]	M ($\times 10^8$ M$_\odot$)	M/L_V (M$_\odot$/L$_\odot$)
KKR 25	dSph	1.93[a] 1.87 1.86	−1.0	M 31	−10.93[a]	23.94[a]			
Phoenix	Tr	0.42[b] 0.86 0.58	0.7	MW	−9.95[c]	24.3[l]	-1.87 ± 0.06[b]	0.31[c]	37
Cetus	dSph	0.78[d] 0.69 0.62	0.3	M 31	−11.34[e]	25.0[e]	−1.9[f]	1.1 ± 0.1[f]	37
Tucana	dSph	0.88[d] 1.34 1.09	−0.2	MW	−9.78[g]	24.95[g]	-1.7 ± 0.2[f]	0.43 ± 0.15[f]	62
And XVIII	dSph	1.36[h] 0.61 0.94	0.4	M 31	−9.7[h]	≤25.6[h]	-1.8 ± 0.1[f]	0.27 ± 0.15[m]	41
KKH 98	Irr	2.49[i] 1.74 2.08	−0.9	M 31	−12.23[j]	22.6[j]	−1.94[j]	0.66[a]	10

[a]This work; [b]Hidalgo et al. (2009); [c]Mateo (1998); [d]Karachentsev et al. (2004); [e]McConnachie & Irwin (2006); [f]Kalirai et al. (2010); [g]Saviane, Held & Piotto (1996); [h]McConnachie et al. (2008); [i]Melbourne et al. (2010); [j]Sharina et al. (2008); [k]Begum et al. (2008); [l]$\Sigma_B = 24.9$ (Lauberts & Valentijn 1989) has been transformed to the V band using $(B - V)_\mathrm{e} = 0.61$ (Prugniel & Heraudeau 1998); [m]$M_{1/2} = 2.7 \times 10^7$ M$_\odot$ (Tollerud et al. 2012) is the mass at the half-light radius of the And XVIII.

The columns are as follows: (1) name of the galaxy; (2) morphological type; (3) distance from the MW, the Andromeda galaxy (M 31) and the centroid of the Local Group (LG) to the galaxy in Mpc; (4) tidal index; (5) main disturber; (6) V-band absolute magnitude of the galaxy; (7) V-band central surface brightness of the galaxy corrected for Galaxy absorption; (8) metallicity [Fe/H] of the galaxy; (9) total mass of the galaxy; (10) V-band total mass-to-luminosity ratio.

of the luminosity function of dSphs. It follows the same relation of surface brightness versus luminosity as the satellites of the MW and M 31. We can expect that KKR 25 traces the same properties as isolated dSphs in the Local Group and has the similar mass and mass-to-light ratio.

In the Local Volume on the scale of a few Mpc, we know only one galaxy comparable with KKR 25 in isolation. This highly isolated dwarf KKH 98 is a normal dIrr galaxy. Hα emission indicates the ongoing SFR, i.e. $\log(\mathrm{SFR}) = -3.5\,\mathrm{M}_\odot\,\mathrm{yr}^{-1}$ (Kaisin, private communication). The observations with GMRT in the framework of Faint Irregular Galaxies GMRT Survey (FIGGS) project (Begum et al. 2008) detect $M_{\mathrm{H\,I}} = 6.46\times10^6\,\mathrm{M}_\odot$ of neutral hydrogen which spreads over 1.4 kpc from the centre of the galaxy. An H I exceeds the optical size of KKH 98 by 3.45 times. A hydrogen mass-to-luminosity ratio $M_{\mathrm{H\,I}}/L_V = 1$ is typical for the dwarf galaxies of given luminosity. Using the data of Begum et al. (2008) ($W_{50} = 20.7\,\mathrm{km\,s}^{-1}$, $i = 46^\circ$, $D_{\mathrm{H\,I}} = 3.8$ arcmin), we estimated the total indicative mass of KKH 98, $M = 6.6\times10^7\,\mathrm{M}_\odot$. The obtained mass is similar to the mass of isolated dSphs. But KKH 98 shows very different morphology, gas and star content. It seems mysterious why the galaxies of similar mass and resembling environment have so different SFHs.

KKR 25 is one of the most isolated galaxies in the vicinity of the Local Group. It does not contain a detectable amount of gas and can be reliably classified as a dSph galaxy. KKR 25 stays far away from any massive galaxy in the Local Volume to be affected by an interaction during its evolution. We can conclude that an evolution of KKR 25 was regulated by star formation in the galaxy itself rather than by its environment. The 'primordial scenario' proposed that dSphs form before the reionization in small haloes, $M < 2\times10^8\,\mathrm{M}_\odot$. Star formation in these haloes is regulated by cooling and feedback processes in the early Universe. Simulations of pre-reionization fossils explain the main properties of dSphs in the Local Group (Bovill & Ricotti 2009). It seems that KKR 25 is the best candidate of such a 'fossil' galaxy (Ricotti & Gnedin 2005).

Tikhonov & Klypin (2009) pointed out that the standard cosmological Λ cold dark matter model predicts a factor of 10 more dwarf haloes in the field than the number of observed dwarf galaxies. Thus, the theory meets the same problem as overabundance of dwarf dark matter haloes in the Local Group, the so-called 'missed satellites' problem. Tikhonov & Klypin (2009) suggested several solutions. One of these implies a significant incompleteness of the observational sample of galaxies. The model predicts 10 times more dwarf galaxies down to a limiting magnitude of $M_B = -12$ than listed in the Karachentsev et al. (2004) sample. Tikhonov & Klypin (2009) proposed that the dSph galaxies are good candidates for this role. Indeed, the sample of dIrrs seems to be complete down to the limit of $M_B = -12$ (Karachentsev et al. 2004). They hold a significant amount of H I gas. An ongoing star formation increases the surface brightness and total luminosity of a galaxy. Therefore, dIrrs are relatively easy to detect. At the same time, dSphs are invisible in blind H I surveys, they have very low surface brightness, which makes them extremely difficult to find. KKR 25 satisfies all these conditions as a first member of population of 'missed' galaxies. It is an isolated, gas-deficient, low surface brightness dSph galaxy. Taking into account only isolated spheroidal galaxies in the Local Group ($N \sim 2$–4), we can roughly estimate the total number of similar systems inside the Local Volume up to 8 Mpc. We could expect to find $N_{\mathrm{t}} \sim 8^3 \times (2\text{–}4) \sim 1000$–2000 objects within the luminosity range $-9.5 > M_V > -11.5$. This number resembles the 1000 'missed' dSphs mentioned by Tikhonov & Klypin (2009). But it is necessary to point out that KKR 25 is one of the most luminous of the known isolated dSphs. It has $M_B \approx -10$ and lies well above the photometric limit of $M_B < -12$. We could expect that other dSph galaxies will be even fainter. Therefore, it seems unlikely that galaxies similar to KKR 25 could solve the problem of 'missed' dwarfs. Anyway, the hunting for dSphs in the field is an important task. Existence of dSph population in voids is the crucial test on models of formation and evolution of dwarf galaxies.

6 CONCLUSIONS

We present a photometric and spectroscopic study of the unique isolated nearby dSph galaxy KKR 25. Let us briefly summarize the results of our study. We have estimated the distance modulus of KKR 25 as $(m-M)_0 = 26.42 \pm 0.07$ mag using the TRGB method. It corresponds to a distance of $D = 1.93 \pm 0.07$ Mpc. The new value is in good agreement with all previous distance measurements.

We have derived a quantitative SFH of the isolated dSph galaxy KKR 25. The SFH was reconstructed using *HST*/WFPC2 images of the galaxy and a resolved stellar population modelling. According to our measurements, 62 per cent of the total stellar mass was formed during the initial burst of star formation occurred about 12.6–13.7 Gyr ago. There are indications of intermediate-age star formation in KKR 25 between 1 and 4 Gyr with no significant signs of metal enrichment for these stars.

A distribution of the stars in the galaxy is well described by an exponential profile with central depression. The exponential scale length is $h = 156^{+12}_{-11}$ pc. The profile extends up to five scale lengths. The size of the depression $R = 170^{+22}_{-30}$ is about the exponential scale length.

We did not confirm the presence of GCs in KKR 25. In fact, the previously selected candidates are background objects, S0 galaxy at $z = 0.34$ and quasar at $z = 0.75$.

The spectroscopy of Hα object in KKR 25 revealed that it is a PN with oxygen abundance $12 + \log(\mathrm{O/H}) = 7.60 \pm 0.07$. We have serendipitously found the first PN in the dSph galaxy outside the Local Group. The search of extraordinary blue stars on the CMD of stellar population gives the perspective method for the selection of PN candidates in distant galaxies.

We have derived the heliocentric velocity of KKR 25 using PN emission lines, $V_{\mathrm{h}} = -79 \pm 9\,\mathrm{km\,s}^{-1}$, and using integrated light of the galaxy, $V_{\mathrm{h}} = -65 \pm 15\,\mathrm{km\,s}^{-1}$.

The 'primordial scenario' of galaxy formation is preferable against tidal stripping mechanism to explain the isolation of KKR 25 and its morphology. Existence of big number of dSphs in the field could explain the overabundance problem in modern simulations. The search for the dSph in voids is a crucial test for the models of formation and evolution of dwarf galaxies.

ACKNOWLEDGMENTS

We are thankful to Dr S. Pustilnik for very useful discussions of our work. We acknowledge the usage of the HyperLEDA data base (http://leda.univ-lyon1.fr). STSDAS is a product of the Space Telescope Science Institute, which is operated by AURA for NASA. The work was supported by the Russian Foundation for Basic Research (RFBR) grant 11-02-00639, Russian–Ukrainian RFBR grant 11-02-90449 and the programme no. 17 'Active processes in galactic and extragalactic objects' of the Department of Physical Sciences of the Russian Academy of Sciences. We acknowledge the support of the Ministry of Education and Science of the Russian Federation, contract 14.740.11.0901.

REFERENCES

Afanasiev V. L., Moiseev A. V., 2005, Astron. Lett., 31, 194
Akaike H., 1974, IEEE Trans. Automatic Control, 19, 716
Banse K., Crane P., Grosbol P., Middleburg F., Ounnas C., Ponz D., Waldthausen H., 1983, Messenger, 31, 26
Barbier-Brossat M., Figon P., 2000, A&AS, 142, 217
Begum A., Chengalur J. N., 2005, MNRAS, 362, 609
Begum A., Chengalur J. N., Karachentsev I. D., Sharina M. E., Kaisin S. S., 2008, MNRAS, 386, 1667
Bovill M. S., Ricotti M., 2009, ApJ, 693, 1859
Boyer M. L., 2008, PhD thesis, Univ. Minnesota
Burnham K. P., Anderson D. R., 2004, Sociological Methods Res., 33, 261
Dalcanton J. J. et al., 2009, ApJS, 183, 67
de Vaucouleurs G., de Vaucouleurs A., Corwin, H. G., Jr, Buta R. J., Paturel G., Fouqué P., 1991, Third Reference Catalogue of Bright Galaxies. Vol. I: Explanations and references. Vol. II: Data for galaxies between 0^h and 12^h. Vol. III: Data for galaxies between 12^h and 24^h. Springer, New York
Dolphin A. E., 2000, PASP, 112, 1383
Fraternali F., Tolstoy E., Irwin M. J., Cole A. A., 2009, A&A, 499, 121
Frew D. J., Parker Q. A., 2010, Publ. Astron. Soc. Australia, 27, 129
Gallart C., Martínez-Delgado D., Gómez-Flechoso M. A., Mateo M., 2001, AJ, 121, 2572
Girardi L., Bressan A., Bertelli G., Chiosi C., 2000, A&AS, 141, 371
Girardi L., Groenewegen M. A. T., Hatziminaoglou E., da Costa L., 2005, A&A, 436, 895
Gonçalves D. R., Magrini L., Leisy P., Corradi R. L. M., 2007, MNRAS, 375, 715
Hidalgo S. L., Aparicio A., Martínez-Delgado D., Gallart C., 2009, ApJ, 705, 704
Huchtmeier W. K., Karachentsev I. D., Karachentseva V. E., 2000, A&AS, 147, 187
Huchtmeier W. K., Karachentsev I. D., Karachentseva V. E., 2003, A&A, 401, 483
Izotov Y. I., Thuan T. X., 2007, ApJ, 665, 1115
Jacoby G. H., 1989, ApJ, 339, 39
Kaisin S. S., Karachentsev I. D., 2008, A&A, 479, 603
Kalirai J. S. et al., 2010, ApJ, 711, 671
Karachentsev I. D. et al., 2001, A&A, 379, 407
Karachentsev I. D., Karachentseva V. E., Huchtmeier W. K., Makarov D. I., 2004, AJ, 127, 2031
Karachentsev I. D., Kashibadze O. G., Makarov D. I., Tully R. B., 2009, MNRAS, 393, 1265
Karachentseva V. E., Karachentsev I. D., Richter G. M., 1999, A&AS, 135, 221
Kass R. E., Raftery A. E., 1995, J. Am. Stat. Assoc., 90, 773
King I., 1962, AJ, 67, 471
Kinney A. L., Calzetti D., Bohlin R. C., McQuade K., Storchi-Bergmann T., Schmitt H. R., 1996, ApJ, 467, 38
Kniazev A. Y., Grebel E. K., Pustilnik S. A., Pramskij A. G., 2007, A&A, 468, 121
Kniazev A. Y., Pustilnik S. A., Zucker D. B., 2008a, MNRAS, 384, 1045
Kniazev A. Y. et al., 2008b, MNRAS, 388, 1667
Lauberts A., Valentijn E. A., eds, 1989, The Surface Photometry Catalogue of the ESO-Uppsala Galaxies. European Southern Observatory, Garching, Germany
Le Borgne D., Rocca-Volmerange B., Prugniel P., Lançon A., Fioc M., Soubiran C., 2004, A&A, 425, 881
Lewis G. F., Ibata R. A., Chapman S. C., McConnachie A., Irwin M. J., Tolstoy E., Tanvir N. R., 2007, MNRAS, 375, 1364
Liddle A. R., 2007, MNRAS, 377, L74
McConnachie A. W., Irwin M. J., 2006, MNRAS, 365, 1263
McConnachie A. W. et al., 2008, ApJ, 688, 1009
Makarov D. I., Makarova L. N., 2004, Astrophysics, 47, 229
Makarov D. I., Karachentsev I. D., Burenkov A. N., 2003, A&A, 405, 951
Makarov D., Makarova L., Rizzi L., Tully R. B., Dolphin A. E., Sakai S., Shaya E. J., 2006, AJ, 132, 2729
Makarova L., Koleva M., Makarov D., Prugniel P., 2010, MNRAS, 406, 1152
Martin N. F., de Jong J. T. A., Rix H., 2008, ApJ, 684, 1075
Mateo M. L., 1998, ARA&A, 36, 435
Melbourne J., Williams B., Dalcanton J., Ammons S. M., Max C., Koo D. C., Girardi L., Dolphin A., 2010, ApJ, 712, 469
Ocvirk P., Pichon C., Lançon A., Thiébaut E., 2006a, MNRAS, 365, 46
Ocvirk P., Pichon C., Lançon A., Thiébaut E., 2006b, MNRAS, 365, 74
Oey M. S., Parker J. S., Mikles V. J., Zhang X., 2003, AJ, 126, 2317
Oke J. B., 1990, AJ, 99, 1621
Paturel G., Petit C., Prugniel P., Theureau G., Rousseau J., Brouty M., Dubois P., Cambrésy L., 2003, A&A, 412, 45
Pickles A. J., 1998, PASP, 110, 863
Plummer H. C., 1911, MNRAS, 71, 460
Prugniel P., Heraudeau P., 1998, A&AS, 128, 299
Prugniel P., Soubiran C., 2001, A&A, 369, 1048
Ricotti M., Gnedin N. Y., 2005, ApJ, 629, 259
Rizzi L., Tully R. B., Makarov D., Makarova L., Dolphin A. E., Sakai S., Shaya E. J., 2007, ApJ, 661, 815
Salpeter E. E., 1955, ApJ, 121, 161
Sánchez-Blázquez P. et al., 2006, MNRAS, 371, 703
Saviane I., Held E. V., Piotto G., 1996, A&A, 315, 40
Saviane I., Exter K., Tsamis Y., Gallart C., Péquignot D., 2009, A&A, 494, 515
Schlegel D. J., Finkbeiner D. P., Davis M., 1998, ApJ, 500, 525
Schwarz G., 1978, Ann. Stat., 6, 461
Sérsic J. L. (ed.), 1968, Atlas de Galaxias Australes. Observatorio Astronomico, Cordoba, Argentina
Sharina M. E. et al., 2008, MNRAS, 384, 1544
Tikhonov A. V., Klypin A., 2009, MNRAS, 395, 1915
Tollerud E. J. et al., 2012, ApJ, 752, 45
Tonry J., Davis M., 1979, AJ, 84, 1511
Tully R. B. et al., 2006, AJ, 132, 729
Vazdekis A., Sánchez-Blázquez P., Falcón-Barroso J., Cenarro A. J., Beasley M. A., Cardiel N., Gorgas J., Peletier R. F., 2010, MNRAS, 404, 1639
Weisz D. R. et al., 2011, ApJ, 739, 5
Wood D. O. S., Churchwell E., 1989, ApJS, 69, 831

This paper has been typeset from a TEX/LATEX file prepared by the author.